Nanoscale

Accepted Manuscript

This article can be cited before page numbers have been issued, to do this please use: D. Ruiz, M. Mizrahi, H. D. Assis Santos, D. Jaque Garcia, C. M. S. Jones, J. Marques-Hueso, C. Jacinto, F.G. Requejo, A. Torres-Pardo, J. M. González-Calbet and B. H. Juarez, *Nanoscale*, 2019, DOI: 10.1039/C9NR02087J.

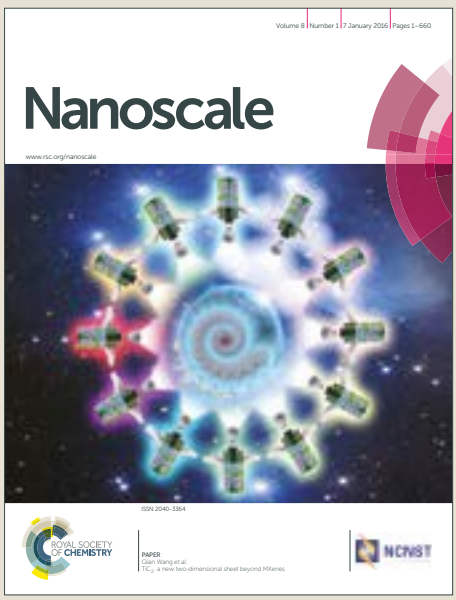




ROYAL SOCIETY OF CHEMISTRY

rsc.li/nanoscale

ROYAL SOCIETY OF CHEMISTRY
View Article Online
DOI: 10.1039/C9NR02087J

Journal Name

ARTICLE

# Synthesis and characterization of $Ag_2S$ and $Ag_2S/Ag_2(S,Se)$ NIR nanocrystals

Received 00th January 20xx,
Accepted 00th January 20xx

DOI: 10.1039/x0xx00000x

www.rsc.org/

Diego Ruiz,[a] Martín Mizrahi,[b] Harrisson D. A. Santos,[c,d], Daniel Jaque,[c] Callum M. S. Jones,[e] José Marqués-Hueso,[e] Carlos Jacinto,[d] Félix G. Requejo,[b] Almudena Torres-Pardo,[f] José M. González-Calbet[f,g] and Beatriz H. Juárez[a,h]

**Syntheses of metal sulfide nanocrystals (NCs) by heat-up routes in the presence of thiols yield NCs arrangements difficult to further functionalize and transfer to aqueous media. By means of different NMR techniques, and exemplified in $Ag_2S$ NCs, a metal-organic polymer formed during the synthesis acting as ligand has been identified as responsible for such aggregation. In this work a new synthetic hot-injection strategy is presented to synthesize $Ag_2S$ NCs easily ligand exchangeable into water. Furthermore, the hot-injection route allows an extra NCs treatment with Se to produce $Ag_2S/Ag_2(S,Se)$ NCs with improved optical properties with respect to the $Ag_2S$ cores, and better resistance to oxidation, as demonstrated by X-Ray absorption experiments.**

## Introduction

Silver sulfide nanocrystals ($Ag_2S$ NCs) have been used in the last years in many research areas ranging from solar cells to biomedicine.[1-7] $Ag_2S$ shows some advantages such as emission in the second biological window (II-BW), where biomolecules and water show less light absorption,[8] and low toxicity compared to other near-infrared (NIR) emitting NCs such as PbS or PbSe.[9] Recently, the use of $Ag_2S$ NCs as ratiometric nanothermometers has also been reported.[10] However, their optical properties are still not fully understood, with reported photoluminescence (PL) emissions from 600 to 1250 nm for similar sized NCs.[11-14]

In general, $Ag_2S$ NCs synthesized in polar solvents show PL emissions much more energetic than those synthesized in non-polar media which emit at 1000-1250 nm (a thorough summary of the reported synthetic routes and their optical properties is given in section S1†). The disparity of results in the syntheses of these NCs demands revision and profuse analyses to rationally understand the formation mechanism of $Ag_2S$ NCs and the relation of the optical properties with their morphology and size.

Furthermore, from the first studies of $Ag_2S$ NCs[15-18] to the most recent ones,[19, 20] the heat-up syntheses using thiols yield NCs arrangements of different sizes that form a non-stable colloid. Indeed, many authors have emphasized the difficulty to further use these metal-sulfide NCs due to a dense surface coating of different thiolated species, thus reducing their potential applications.[21-25] The disaggregation of such NCs arrangements is key to facilitate ligand exchange procedures and solution processability. In this work, we shed light on the chemistry behind the synthesis of $Ag_2S$ NCs using silver (I) diethyldithiocarbamate (AgDDTC) and 1-dodecanethiol (DDT) and propose a hot-injection route to avoid the formation of such arrangements. This route yields isolated and stable $Ag_2S$ NCs that can be further used as seeds to obtain $Ag_2S/Ag_2(S,Se)$ NCs with improved optical properties upon a Selenium treatment. As far as the authors know, no previous similar NCs have been described. [19,22, 26] The obtained hot-injection $Ag_2S$ and $Ag_2S/Ag_2(S,Se)$ NCs are easily transferable to water by simple ligand exchange procedures.

## Results and discussion

[a] IMDEA Nanoscience, Faraday 9, Campus de Cantoblanco, 28049, Madrid, Spain.
[b] Instituto de Investigaciones Fisicoquímicas Teóricas y Aplicadas (INIFTA), CONICET and FCE, UNLP, CC/16, suc 4 , 1900, La Plata, Argentina.
[c] Fluorescence Imaging Group, Materials Physics Department, Universidad Autónoma de Madrid, Campus Cantoblanco, 28049, Madrid, Spain.
[d] Group of Nano-Photonics and Imaging, Instituto de Física, Universidade Federal de Alagoas, 57072-900 Maceió-AL. Brazil
[e] Institute of Sensors, Signals and Systems, Heriot-Watt University, Edinburgh, EH14 4AS, United Kingdom.
[f] Inorganic Chemistry department, Chemical Sciences Faculty, Universidad Complutense de Madrid, 28040, Madrid, Spain.
[g] ICTS National Center for Electronic Microscopy, Universidad Complutense, 28040, Madrid, Spain.
[h] Department of Applied Physical Chemistry and Condensed Matter Physics Center (IFIMAC), Universidad Autónoma de Madrid, 28049 Madrid, Spain.
†Electronic Supplementary Information (ESI) available.

Fig 1a shows a TEM image of $Ag_2S$ NCs produced by a heat-up route in non-polar media using AgDDTC and DDT (route A, section S2†), where highly ordered aggregates are formed. These NCs have been previously studied by advanced microscopy and show a Ag-rich core.[10] So far, these aggregates have been treated as self-assembled NCs due to the high monodispersity of the samples and the high degree of interdigitation and interaction between NCs.[18, 27] Figure 1b shows the result of the here proposed hot-injection route (route B, section S2† for details), where, in contrast, isolated NCs are evident. These NCs consist of pure $Ag_2S$ NCs, as can be concluded from Figure 1c showing the HRTEM image of four NCs. The distances and angles obtained from their FFT analysis correspond to monoclinic acanthite $Ag_2S$ phase ($\alpha$-$Ag_2S$). Figures 1E-F show the elemental mapping distribution of the HAADF-STEM image of Figure 1D.

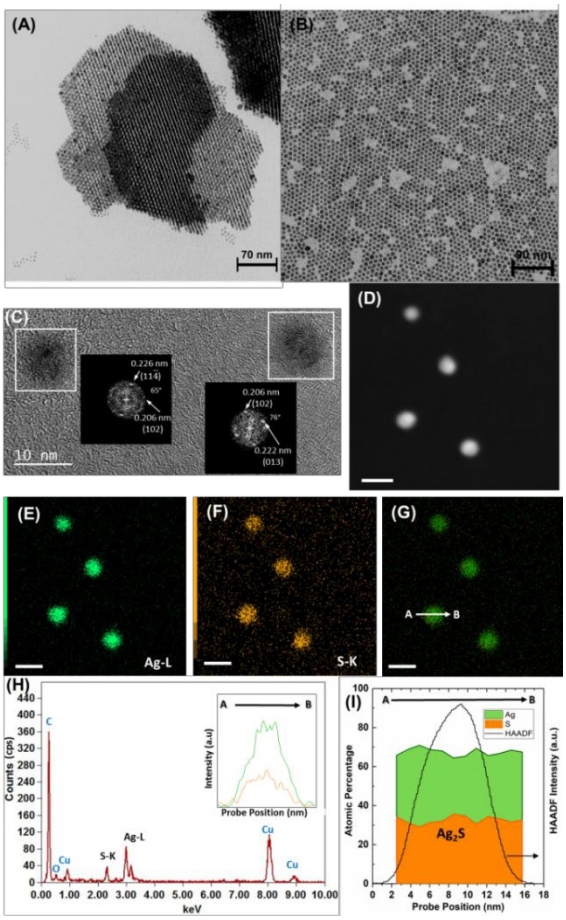


**Fig.1** (A) TEM images of $Ag_2S$ NCs aggregates produced by heat-up (route A, S2†) and (B) disaggregated NCs obtained by the hot injection route (route B, S2†). (C) HRTEM images of $Ag_2S$ NCs. Insets show the FFT performed on each NCs. D) Low magnification HAADF-STEM of $Ag_2S$ NCs. (E-G) EDS elemental mapping showing the spatial distribution of e) Ag (green), (F) S (orange), and (G) Ag and S of the set of NCs shown in (D). (H) Representative EDS spectrum of a NC. The corresponding X-ray intensity profiles extracted from the white arrow marked in image (G) are shown as an inset. (I) Atomic percentage of the previous intensity profile revealing $Ag_2S$ composition for the NCs.

The homogeneous distribution of Ag and S is revealed by the analysis of the EDS spectrum (inset of Figure 1H) across the NC marked with an arrow in Figure 1G. The corresponding X-Ray intensity profile shown in Figure 1H as inset, as well as the quantification of the intensity profile shown in Figure 1I, confirm the presence of NCs with a composition close to the stoichiometric $Ag_2S$.

The isolation of the NCs-aggregates has been possible by gaining insights into the chemistry of the NCs' formation by Nuclear Magnetic Resonance, NMR. Figure 2 compares the $^1$H NMR spectra of (A) DDT, (B) a dispersion of $Ag_2S$ NCs produced by heat-up route A with DDT and (C) silver (I) dodecanethiolate (Ag-DCT), a metal-organic polymeric product synthesized based on a previously reported recipe.[28]

As evidenced, most of the signals present in the $Ag_2S$ NCs spectrum (B) are shared by the metal-organic polymeric product signals (C). The signals related to the protons in the $\alpha$ and $\beta$ positions to the thiol group in the DDT spectrum (A) are at $\delta = 2.50$ ppm and $\delta = 1.60$ ppm, respectively (marked in grey). Bound DDT to colloidal quantum dots of different composition or $CuInS_2$ NCs is reported as a broad peak between 2.5 and 2.7 ppm. [23, 29]

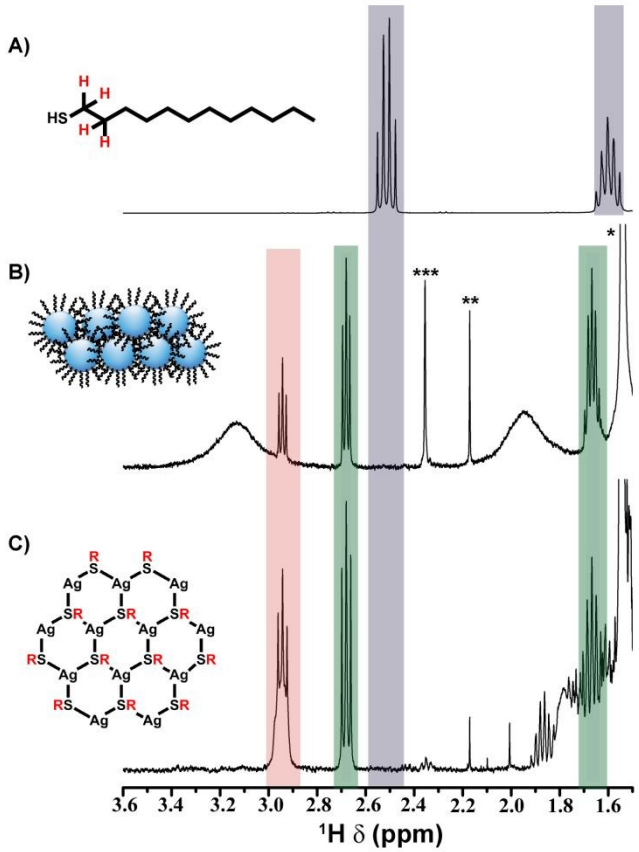


**Fig.2** $^1$H NMR spectra of A) DDT, B) NCs synthesized by heat-up route A and C) the reaction intermediate (silver (I) dodecanethiolate). The signals marked in green correspond to dodecyl disulphide, in red to silver (I) dodecanethiolate and in grey to dodecanethiol. Signals marked with three, two and one star (*) correspond to residual toluene, acetone and water, respectively. Insets depict DDT (A), NCs-aggregates by the effect of Ag-DCT (B) and the polymer, Ag-DCT(C).

The absence of these signals in the NCs spectrum (B) discards the presence of DDT, free or anchored to the NCs surface. The signals at 2.70 ppm and 1.65 ppm (marked in green), which are present both in the polymer (Ag-DCT) and the NCs spectra are assigned to dodecyl disulfide, a well-known side product in the synthesis of metal sulfide NCs produced upon the oxidation of DDT.[21, 30]

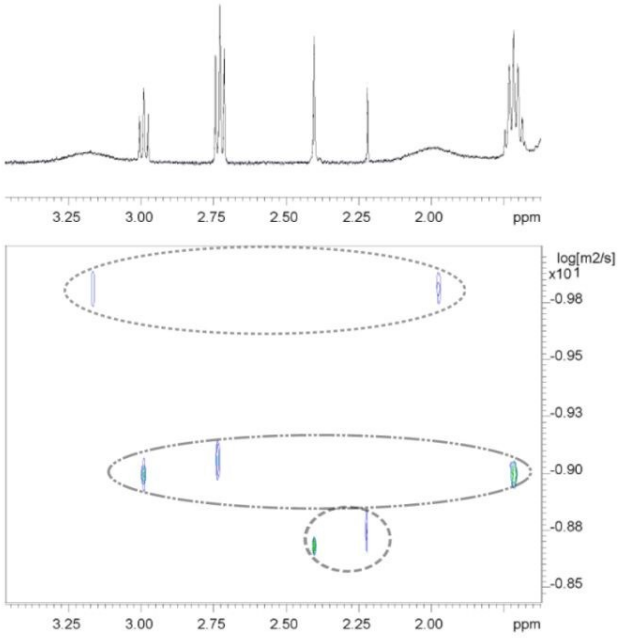


**Fig.3** DOSY spectrum of NCs synthesized by route A. From bottom to top, three sets of signals can be distinguished, corresponding to solvents, non-anchored species and anchored Ag-DCT to the NC surface, respectively.

Likewise, the Ag-DCT and the NCs spectra share a triplet signal at 2.95 ppm related to the $\alpha$-protons to the thiol group in the polymer. This signal, along with those related to dodecyl disulfide, are narrow and show multiplicity, suggesting that they are species that can be forming part of the ligand shell but are not directly anchored to the surface. In contrast, in the spectra of the NCs, two additional broad signals centered at 1.95 and 3.10 ppm can be observed. Their width suggest a strong interaction with the NCs surface, as confirmed by the Diffusion-Ordered Spectroscopy (DOSY) spectrum shown in Figure 3. In this spectrum two different sets of signals can be distinguished (apart from those coming from solvents): signals with diffusion coefficients far from bound species ( $\sim 1 \cdot 10^{-9}$ $m^2/s$) and two signals with diffusion coefficients of $1.4 \cdot 10^{-10}$ $m^2/s$, a reasonable value for tightly bound ligands to NCs surfaces.[31] The first set of signals is related to free Ag-DCT (at $\delta$=2.95 ppm) and dodecyl disulphide (at $\delta$ = 1.65 and $\delta$ = 2.70 ppm). The second set of signals at $\delta$= 3.10 and $\delta$ = 1.95 ppm is thus assigned to the Ag-DCT polymer. Applying the Stokes-Einstein relation,[32] the hydrodynamic diameter of these species is calculated to be 5 nm, close to the size of the NCs observed in TEM images (details in section S3†).

These findings, along with the aggregation observed in TEM images indicate that the main species anchored to the NCs surface is the Ag-DCT polymer. Further evidences of the presence of this polymer during the synthesis of the $Ag_2S$ NCs produced by route A is given by TEM and XRD measurements (Section S4†). As previously reported, this polymer presents a lamellar structure, in which the silver atoms are located in plane, while the aliphatic chains of DDT are oriented perpendicular and interacting through van der Waals forces forming stacks of these lamellae with high thermal stability.[28, 33] The ability of metallic thiolates to embed other metal chalcogenide NCs has been observed for $Cu_{2-x}S$ obtained from copper dodecanethiolate and octanethiolate[29] and recently, their role as templates for the formation of $Cu_2Se$ and $Ag_2Se$ nanowires through the calcination of their columnar phase, has also been reported.[34] Thus, it seems plausible that Ag-DCT acts as a template in the here described synthesis of $Ag_2S$ by heat-up route A.

Once the presence of this polymer on the surface of the NCs is confirmed, different synthetic strategies were followed to remove it and turn the NCs solution processable. It was found that a combination of toluene and sulfur in oleylamine (OLA) is key to obtain isolated NCs as those shown in Figure 1b. The combination of these products was chosen because, on the one hand, toluene near its boiling point is the only known solvent for Ag-DCT.[35] On the other hand, the injection of sulfur in OLA at 100°C rapidly produces $H_2S$,[36] causing the fast formation of metal sulfide NCs upon injection. The role of OLA in this synthesis is not only the activation of sulfur to produce $H_2S$, but also to define the final surface chemistry of the NCs, as evidenced in the $^1$H NMR spectra shown in Figure 4, where the spectrum of OLA (Figure 4A) is compared to that of NCs produced by route B (Figure 4B). Indeed, OLA is found to bind to the surface of these NCs, as suggested by the broad peaks at $\delta$ = 5.3 ppm and $\delta$ = 2.0 ppm in the $^1$H NMR spectrum marked in blue (Figure 4B).

In these samples we can also observe narrow signals from dodecyl disulfide and free Ag-DCT, suggesting that these species might be intercalated between the anchored OLA ligands. However, no evidence for the broad signal at $\delta$ = 3.10 ppm can be distinguished, confirming the absence of anchored Ag-DCT to the NCs surface.

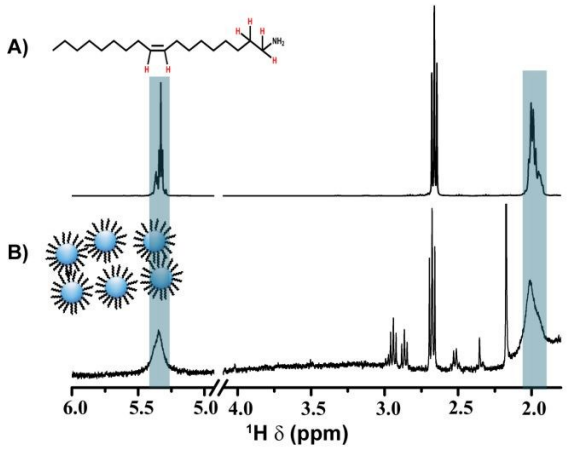


**Fig.4** $^1$H NMR spectrum of a) Oleylamine and b) NCs synthesized by the hot injection route (route B in section S2†).

View Article Online
DOI: 10.1039/C9NR00073



Due to the presence of OLA on the NCs surface, the $Ag_2S$ NCs obtained by this novel route (route B), free of the Ag-DCT polymer as ligand, are easily ligand-exchangeable with water-soluble ligands like thiol-modified polyethylene glycol, providing bright water soluble NCs stable in solution for months (see section S5† for further TEM (Figure S5.1) and optical characterization of $Ag_2S$ NCs in tetrachloroethylene (TCE) and water (Figure S5.2)). The evidence for a better ligand exchange process due to the presence of OLA passivating the NCs was obtained by ICP-MS. The results are shown on Table 1.

| | $Ag^+$ mass in chloroform (mg) | $Ag^+$ mass in water (mg) | Yield (%) |
|---|---|---|---|
| **Route A NCs** | 1.923±0.008 | 0.282±0.005 | 15 |
| **Route B NCs** | 1.536±0.004 | 1.022±0.001 | 67 |

**Table 1.** Amount of $Ag_2S$ NCs transferred to water depending on the synthetic procedure.

Table 1 shows that when route A NCs are exposed to a ligand exchange procedure, only 15% of the silver mass in the NCs is transferred to water. However, when route B NCs are exposed to the same ligand exchange procedure, 67% of them end up in the aqueous phase. Thus, it is clear that the elimination of the dense coating of the polymer is a major advantage for post-reaction treatments of the NCs. Disaggregation and good colloidal stability provided by this route allows not only an easier ligand exchange, but also further control of their optical properties by post synthetic procedures, as shown in Figure 5A, showing the absorption and emission spectra of $Ag_2S$ NCs and NCs treated with Se, $Ag_2S/Ag_2(S,Se)$ NCs. In particular, the addition of Se in a quantity equivalent to the growth of roughly a monolayer of $Ag_2Se$ on the surface of the NCs (through a solution of Se@TOP, see details in S2†) yields NCs with improved optical properties while maintaining their size dispersion and stability. The improved optical properties is presumably due to the passivation of surface trap states.

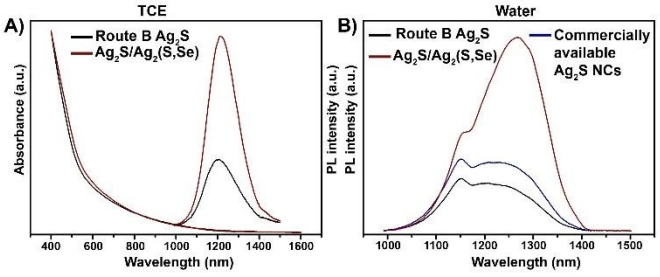


**Fig.5** A) Absorption and photoluminescence of the as-synthesized $Ag_2S$ (black) and $Ag_2S/Ag_2(S,Se)$ NCs (red) for the same value of O.D. = 0.1 at $\lambda_{exc}$ = 822 nm in tetrachloroethylene, TCE. B) Comparison between the PL of commercially available NCs (blue) and the ones synthesized in this work: $Ag_2S$ (black) and $Ag_2S/Ag_2(S,Se)$ (red) at O.D.= 0.1 at $\lambda_{exc}$ = 822 nm in water.

Furthermore and importantly, according to its $^1H$ NMR spectrum (Figure S6.1†), this growth step in the presence of Se does not modify the ligand sphere of the NCs, allowing for similar ligand exchange procedures as the one developed for the previously described $Ag_2S$ NCs. (Section S6† for TEM and optical characterization). The addition of more Se does not generate an improvement in their optical properties but lowers their colloidal stability due to unreacted Se@TOP.

The measurement of the photoluminescence quantum yield (PLQY) in the NIR region is challenging due to the lesser sensitivity of the infrared detectors compared to the visible range ones, and due to the instability of the NIR emitting dyes like those commonly used (IR-125 and IR-26).[35] Moreover, the PLQY of IR-26 that is taken as standard, has been recently reviewed after accurate measurements with an integrating sphere.[37, 38] This method has the advantage of measuring directly the amount of absorbed and emitted photons by the whole sample, which results in more accurate values than other methods such as dynamics measurements[39] because it considers physical limitations like reabsorption.[40] For this reason, the absolute PLQY of all the samples synthesized in this work was measured using an integrating sphere. Details of the procedure are described elsewhere.[40]

The PLQY of the here studied samples in TCE is 2.5% (for route A NCs), 0.24% (for route B NCs) and 0.65% for $Ag_2S/Ag_2(S,Se)$ NCs. These differences between route A (heat-up) and route B (hot-injection) NCs may be related to different factors including different synthesis temperature (around 200°C for heat-up NCs and 100°C for hot-injection ones), NCs size (smaller in general for heat-up NCs) and ligand density. As comparison, in the case of the NCs synthesized by route A the reported PLQY obtained after ligand exchange is around 10-15% when measured using the dye IR-26 (see Table 1, section S1†). In our case, measured with the integrating sphere, similar samples gave a QY in tetrachloroethylene (TCE) of 2.5%, which is around 5 times lower than the one obtained using the dye, making it difficult to compare the yield from these two different methods.

For this reason, in order to confirm the potential use of the NCs in aqueous media, their PL was compared to commercially available $Ag_2S$ NCs in water. As shown in Figure 5B for the same value of O.D. (0.1) and excited at the same wavelength (822 nm) the PL emission intensity of water soluble $Ag_2S/Ag_2(S,Se)$ NCs is more than double of commercial ones, while water soluble $Ag_2S$ (route B) show less intensity. While higher values are desirable, recent works show that the PLQY of these NCs are sufficient to perform optical studies *in vivo*.[41] Thus, the benefit of the here described $Ag_2S/Ag_2(S,Se)$ NCs is twofold: Improved optical properties with respect to $Ag_2S$ ones and the possibility to transfer into water much higher amounts of NCs in one single procedure, saving ligand and time. This allows the production of concentrated samples with higher PL signal than commercially available NCs from one single batch.

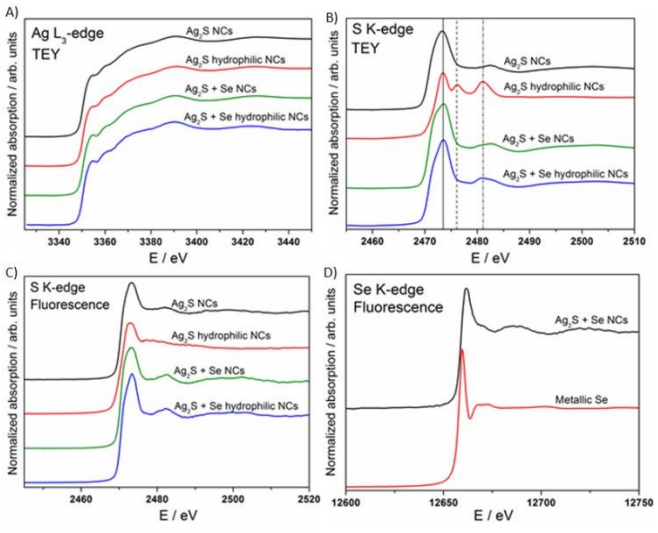


**Fig.6** XANES spectra of the studied $Ag_2S$ samples before and after ligand exchange, and with and without Se, performed in TEY mode at the Ag $L_3$-edge (A) and S K-edge (B). (C) XANES spectra of the studied $Ag_2S$ samples before and after ligand exchange, and with and without Se, performed in fluorescence mode at the S K-edge. (D) XANES spectra of the $Ag_2S_{1-x}Se_x$ sample, performed in fluorescence mode at the Se K-edge

In order to elucidate the incorporation of Se in the $Ag_2S$ matrix (its location on the surface or in the volume), EDX and EELS studies were performed. However, due to the low quantity of Se in the samples, EDX mapping was not able to properly resolve the structure. For this reason, XAS studies including XANES (X-Ray Absorption Near Edge Structure) and EXAFS (Extended X-Ray Absorption Fine Structure), were performed.

The results at the Ag $L_3$- and S K-edges can be seen in Figure 6A and 7B for $Ag_2S$ NCs before and after ligand exchange and with and without Se. As can be seen in Figure 6A, the XANES spectra at the Ag $L_3$-edge in Total Electron Yield (TEY) mode, are almost identical in all samples. The same results are obtained from the signal acquired in fluorescence mode (not shown here). The shape of these spectra is also similar to those that present for reference materials, $Ag_2S$ and $Ag_2Se$,[42] and for silver NPs capped with dodecanethiol.[43] Thus, a clear identification of the formed species is not straightforward in the silver edge.

XANES spectra at the S K-edge taken in TEY mode (Figure 6B), show a main contribution at 2473 eV (vertical solid line) associated to the presence of $S^{-2}$ in all samples. $Ag_2S$ NCs after ligand exchange (denoted as $Ag_2S$ hydrophilic NCs, red line), present other two resonances at 2476 eV (vertical dashed line) and 2481 eV (vertical dashed-dotted line), corresponding to the presence of sulfur with valence states +4, and a mixture of +5 and +6, respectively. It is worth to note that these resonances do not appear in the hydrophilic sample treated with Se ($Ag_2S/Ag_2(S,Se)$ NCs transferred to water) and were not observed in any of the samples when the absorption signal is taken in fluorescence mode (Figure 6C), being in this last case all the signals measured corresponding to $S^{-2}$. TEY mode is sensitive to the surface atom's state, while the fluorescence mode is volume sensitive, giving an averaged information from the whole NC. The comparison of both spectra shows that the Se atoms are located on the surface of the NCs, preventing the oxidation of S when the sample is in aqueous media. This extra layer is not only favouring the PLQY of the NCs but is also acting as a protection layer that isolates their surface from the air oxidation improving their long-term stability. However, the XANES spectra do not present any information about the chemical state of Se in the Ag and S absorption edges due to the difference in the concentration of Ag and S compared to the one of Se. For this reason, XAS measurements (XANES and EXAFS) were performed at the Se K-edge. The XANES region performed in fluorescence mode (Figure 6D) for $Ag_2S$ NCs treated with Se@TOP show all the features present in the spectrum corresponding to the $Ag_2Se$ reference sample,[44] and completely different from the spectrum of metallic Se, so the presence of $Se^0$ covering the NCs can be discarded.

The Se atomic distribution in the Se treated NCs was analysed by probing the local structure around Se atoms by EXAFS. This technique provides structural information of both homogeneous and non-homogeneous nanomaterials by the analysis of the fitted averaged coordination numbers and interatomic distances.[45] Figure 7A shows the magnitude of the Fourier Transform (FT) of the EXAFS oscillation obtained at the Se K-edge, and simulated spectra using FEFF code[46] for $Ag_2Se$ and $SeS_2$. The FT of the sample presents two principal peaks at 1.8 Å and 2.5 Å (without phase correction).

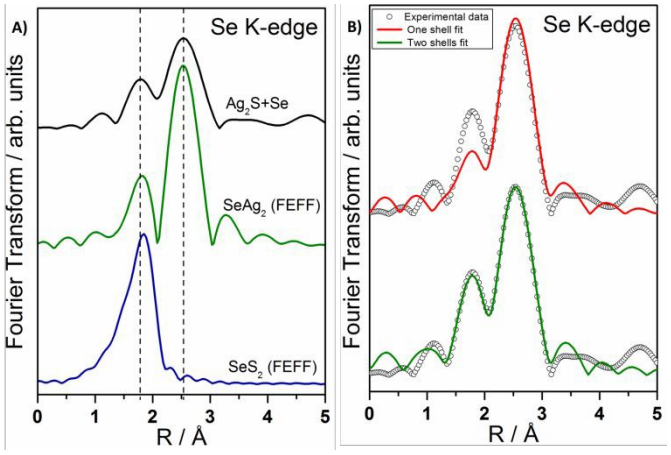


**Fig.7** A) $k^2$-weighted Fourier Transform of the EXAFS oscillation for the $Ag_2S_{1-x}Se_x$ NCs (black line), simulated spectra obtained using the FEFF code for $Ag_2Se$ (green line) and $SeS_2$ (blue line). B) $k^2$-weighted Fourier Transform of the EXAFS oscillation for $Ag_2S/Ag_2(S,Se)$ NCs (circles), together with the fitting models proposed: one shell Se-Ag (red line) and two shells Se-Ag and Se-S (green line).

These contributions are approximately in the same positions that the obtained for the $Ag_2Se$ structure, in accordance with the XANES results. We can observe a difference in the intensity ratio between these peaks, being roughly 1/2 for the studied sample, and roughly 1/3 for the theoretical structure of $Ag_2Se$ (see Figure 7A). This difference can be attributed to the presence of some S atoms in the neighbourhood of Se.

To verify this hypothesis, two fit models were proposed; the first one considers only one shell around the Se atoms composed by atoms of Ag. The result of the fit is shown in Figure 7B (in red), and as it can be seen, its quality is not good enough, especially for the first peak. The second model, adding a new coordination shell for Se, containing S atoms, shows a much better fitting result (Figure 7B (in green) and Table S7†).

The $Ag_2Se$ alloy has seven Ag atoms as first neighbours of the Se ones, with interatomic distances ($R_{Se-Ag}$) between 2.7 and 2.9 Å. For the sample treated with Se, the average coordination number ($N_{Se-Ag}$) obtained from the fit ($N_{Se-Ag}$= 2.8, see Table S7†) is lower than expected (i.e. seven Ag atoms), and also the presence of some S atoms in the structure is needed to improve the quality of the fit (Figure 7B). The presence of some S atoms in the structure would lead to a reduction in the $N_{Se-Ag}$, but this could not fully explain the reduction found. On the other hand, the reduction in the $N_{Se-Ag}$ can be a consequence of both, the nanometric size of the NCs and the superficial location of Se in the NCs. Indeed, those Se atoms on the surface of a NC contribute with a lower $N_{Se-Ag}$ that those in the bulk. Thus, for a NC of about 8 nm of diameter (according to TEM measurements, see Figure S6.4†), a reduction of less than a 5% in the $N_{Se-Ag}$ can be expected. Since in these NCs the decrease is higher (60%), to explain this additional reduction for the $N_{Se-Ag}$, it is necessary that the Se atoms form a $Ag_2(S,Se)$ structure, preferably in a thin layer (less than 1 nm) over the surface of the $Ag_2S$ NCs.

## Conclusions

In conclusion, NMR studies have allowed identifying the presence of silver (I) dodecanethiolate, a polymer that forms during the synthesis of $Ag_2S$ NCs by heat-up routes in the presence of thiols. This route produces well-ordered NCs aggregates with poor colloidal stability and reduced processability, as this polymer hinders effective ligand-exchange procedures to make the NCs water-soluble.

The development of a novel synthetic route allows obtaining $Ag_2S$ NCs with increased versatility allowing for much more efficient ligand exchange procedures, and further growth of a $Ag_2(S,Se)$ outer layer, as resolved by advance synchrotron XAS spectroscopy. $Ag_2S/Ag_2(S,Se)$ NCs show improved chemical stability compared to core-only NCs and improved optical properties compared to commercially available $Ag_2S$ NCs.

## Authorship

Diego Ruiz is the main contributor to this work and performed synthesis, steady-state optical characterization, XRD, TEM and NMR experiments under the supervision of Beatriz H. Juarez, who led the research. Martín Mizrahi and Felix G. Requejo performed the synchroton measurements and contributed with the X-ray Absorption Spectroscopy information. Callum M. S. Jones and José Marqués-Hueso performed the quantum yield measurements in an integration sphere. Almudena Torres-Pardo and José M. González-Calbet were in charge of the advanced HRTEM inspections in the aberration corrected microscope. Harrisson D. A. Santos performed optical characterization under the supervision of Daniel Jaque and Carlos Jacinto. All authors contributed to the written text.

## Conflicts of interest

The authors declare no competing financial interests.

## Acknowledgements

Work supported by the Spanish Ministry of Economy and Competitiveness under Projects #MAT2016-75362-C3-1-R, #FIS2015-67367-C2-1-P, and MAT2017-85617-R. COST Action CM1403 and UAM-Santander Yerun Projects are also acknowledged. This work has also received support from Comunidad Autónoma de Madrid through B2017/BMD-3867RENIM-CM. BHJ acknowledges financial support from the Spanish Ministry of Economy and Competitiveness, through the "Maria de Maeztu" (IFIMAC) and "Severo Ochoa" (IMDEA Nanoscience) Programmes for Units of Excellence in R&D. H.D.A.S. is supported by a graduate studentship from CAPES (Coordenadoria de Aperfeiçoamento de Pessoal de Ensino Superior, Brazil) and by a PDSE-CAPES program developed at Universidad Autónoma de Madrid, Spain, Project PDSE No. 88881.134486/2016-01. C.J. is supported by a scholarship in Research Productivity 1C from CNPq (Conselho Nacional de Densenvolvimento Científico e Tecnológico, Brazil) under Nr. 304967/2018-1. The authors would like to thank the NMR service of the Universidad Autónoma de Madrid for the analysis and discussion of the results.

XAFS experiments were partially supported by Projects XAFS2 20170359 and SXS-20180281 (LNLS, Campinas, Brazil). M.M., and F.G.R. acknowledge CONICET and ANPCYT (Project PICT 2015-2285).

## References

1. T. Yang, Y. a. Tang, L. Liu, X. Lv, Q. Wang, H. Ke, Y. Deng, H. Yang, X. Yang, G. Liu, Y. Zhao and H. Chen, *ACS Nano*, 2017, **11**, 1848-1857.
2. S. Li, L. Xu, M. Sun, X. Wu, L. Liu, H. Kuang and C. Xu, *Advanced Materials*, 2017, **29**, 1606086.
3. X. Zhang, M. Liu, H. Liu and S. Zhang, *Biosensors and Bioelectronics*, 2014, **56**, 307-312.
4. G. Chen, F. Tian, Y. Zhang, Y. Zhang, C. Li and Q. Wang, *Advanced Functional Materials*, 2013, **24**, 2481-2488.



 

5. J. Amaya Suárez, J. J. Plata, A. M. Márquez and J. Fernández Sanz, *The Journal of Physical Chemistry A*, 2017, **121**, 7290-7296.
6. M. Jagadeeswararao, A. Swarnkar, G. B. Markad and A. Nag, *The Journal of Physical Chemistry C*, 2016, **120**, 19461-19469.
7. S. Lin, Y. Feng, X. Wen, T. Harada, T. W. Kee, S. Huang, S. Shrestha and G. Conibeer, *The Journal of Physical Chemistry C*, 2016, **120**, 10199-10205.
8. A. M. Smith, M. C. Mancini and S. Nie, *Nature Nanotechnology*, 2009, **4**, 710-711.
9. F. Hu, C. Li, Y. Zhang, M. Wang, D. Wu and Q. Wang, *Nano Research*, 2015, **8**, 1637-1647.
10. D. Ruiz, B. del Rosal, M. Acebrón, C. Palencia, C. Sun, J. Cabanillas-González, M. López-Haro, A. B. Hungría, D. Jaque and B. H. Juarez, *Advanced Functional Materials*, 2017, **27**, 1604629.
11. Y. Du, B. Xu, T. Fu, M. Cai, F. Li, Y. Zhang and Q. Wang, *Journal of the American Chemical Society*, 2010, **132**, 1470-1471.
12. R. Gui, A. Wan, X. Liu, W. Yuan and H. Jin, *Nanoscale*, 2014, **6**, 5467-5473.
13. Y. Zhang, Y. Liu, C. Li, X. Chen and Q. Wang, *The Journal of Physical Chemistry C*, 2014, **118**, 4918-4923.
14. R. Ahmad, R. Srivastava, H. Bhardwaj, S. Yadav, V. Nand Singh, S. Chand, N. Singh and S. Sapra, *ChemistrySelect*, 2018, **3**, 5620-5629.
15. L. Motte, F. Billoudet and M. P. Pileni, *The Journal of Physical Chemistry*, 1995, **99**, 16425-16429.
16. A. Taleb, C. Petit and M. P. Pileni, *The Journal of Physical Chemistry B*, 1998, **102**, 2214-2220.
17. L. Motte, F. Billoudet, E. Lacaze, J. Douin and M. P. Pileni, *The Journal of Physical Chemistry B*, 1997, **101**, 138-144.
18. M. P. Pileni, L. Motte, F. Billoudet, J. Mahrt and F. Willig, *Materials Letters*, 1997, **31**, 255-260.
19. S. Shen, Y. Zhang, L. Peng, Y. Du and Q. Wang, *Angewandte Chemie International Edition*, 2011, **50**, 7115-7118.
20. Z. Zhuang, X. Lu, Q. Peng and Y. Li, *Chemistry – A European Journal*, 2011, **17**, 10445-10452.
21. M. J. Turo and J. E. Macdonald, *ACS Nano*, 2014, **8**, 10205-10213.
22. R. Xie, M. Rutherford and X. Peng, *Journal of the American Chemical Society*, 2009, **131**, 5691-5697.
23. M. Gromova, A. Lefrançois, L. Vaure, F. Agnese, D. Aldakov, A. Maurice, D. Djurado, C. Lebrun, A. de Geyer, T. U. Schülli, S. Pouget and P. Reiss, *Journal of the American Chemical Society*, 2017, **139**, 15748-15759.
24. Z. Pan, I. Mora-Seró, Q. Shen, H. Zhang, Y. Li, K. Zhao, J. Wang, X. Zhong and J. Bisquert, *Journal of the American Chemical Society*, 2014, **136**, 9203-9210.
25. C. H. M. van Oversteeg, F. E. Oropeza, J. P. Hofmann, E. J. M. Hensen, P. E. de Jongh and C. de Mello Donega, *Chemistry of Materials*, 2019, **31**, 541-552.
26. M. Bernechea, N. C. Miller, G. Xercavins, D. So, A. Stavrinadis and G. Konstantatos, *Nature Photonics*, 2016, **10**, 521.
27. L. Motte, F. Billoudet, E. Lacaze and M.-P. Pileni, *Advanced Materials*, 1996, **8**, 1018-1020.
28. I. G. Dance, K. J. Fisher, R. M. H. Banda and M. L. Scudder, *Inorganic Chemistry*, 1991, **30**, 183-187.
29. M. Acebrón, J. F. Galisteo-López, D. Granados, J. López-Ogalla, J. M. Gallego, R. Otero, C. López and B. H. Juárez, *ACS Applied Materials & Interfaces*, 2015, **7**, 6935-6945.
30. P. Reiss, M. Carrière, C. Lincheneau, L. Vaure and S. Tamang, *Chemical Reviews*, 2016, **116**, 10731-10819.
31. B. Fritzinger, R. K. Capek, K. Lambert, J. C. Martins and Z. Hens, *Journal of the American Chemical Society*, 2010, **132**, 10195-10201.
32. Z. Hens and J. C. Martins, *Chemistry of Materials*, 2013, **25**, 1211-1221.
33. Z. Ye, L. P. de la Rama, M. Y. Efremov, J.-M. Zuo and L. H. Allen, *Dalton Transactions*, 2016, **45**, 18954-18966.
34. W. Bryks, S. C. Smith and A. R. Tao, *Chemistry of Materials*, 2017, **29**, 3653-3662.
35. A. A. Levchenko, C. K. Yee, A. N. Parikh and A. Navrotsky, *Chemistry of Materials*, 2005, **17**, 5428-5438.
36. J. W. Thomson, K. Nagashima, P. M. Macdonald and G. A. Ozin, *Journal of the American Chemical Society*, 2011, **133**, 5036-5041.
37. O. E. Semonin, J. C. Johnson, J. M. Luther, A. G. Midgett, A. J. Nozik and M. C. Beard, *The Journal of Physical Chemistry Letters*, 2010, **1**, 2445-2450.
38. S. Hatami, C. Würth, M. Kaiser, S. Leubner, S. Gabriel, L. Bahrig, V. Lesnyak, J. Pauli, N. Gaponik, A. Eychmüller and U. Resch-Genger, *Nanoscale*, 2015, **7**, 133-143.
39. A. Penzkofer, O. Lammel and T. Tsuboi, *Optics Communications*, 2002, **214**, 305-313.
40. A. Boccolini, J. Marques-Hueso, D. Chen, Y. Wang and B. S. Richards, *Solar Energy Materials and Solar Cells*, 2014, **122**, 8-14.
41. B. del Rosal, D. Ruiz, I. Chaves-Coira, B. H. Juárez, L. Monge, G. Hong, N. Fernández and D. Jaque, *Advanced Functional Materials*, 2018, **28**, 1806088.
42. Y. L. Mikhlin, G. A. Pal'yanova, Y. V. Tomashevich, E. A. Vishnyakova, S. A. Vorobyev and K. A. Kokh, *Journal of Physics and Chemistry of Solids*, 2018, **116**, 292-298.
43. J. D. Padmos and P. Zhang, *The Journal of Physical Chemistry C*, 2012, **116**, 23094-23101.
44. E. Nakazawa, T. Ikemoto, A. Hokura, Y. Terada, T. Kunito, T. Yamamoto, T. K. Yamada, F. C. W. Rosas, G. Fillmann, S. Tanabe and I. Nakai, *Journal of Environmental Monitoring*, 2011, **13**, 1678-1686.
45. A. I. Frenkel, A. Yevick, C. Cooper and R. Vasic, *Annual Review of Analytical Chemistry*, 2011, **4**, 23-39.
46. J. J. Rehr, J. J. Kas, F. D. Vila, M. P. Prange and K. Jorissen, *Physical Chemistry Chemical Physics*, 2010, **12**, 5503-5513.